Solubility of 1:1 Alkali Nitrates and Chlorides in Near-Critical and Supercritical Water

Ingo Leusbrock,*,† Sybrand J. Metz,† Glenn Rexwinkel,‡ and Geert F. Versteeg‡,§

Wetsus, Centre of Excellence for Sustainable Water Technologies, Agora 1, 8900 CC Leeuwarden, The Netherlands, PROCEDE TWENTE B.V., 7544 GG Enschede, The Netherlands, and University of Groningen, Stratingh Institute for Chemistry and Technology, Chair of Process Technology, 9747 AG Groningen, The Netherlands

To increase the available data on systems containing supercritical water and inorganic compounds, an experimental setup was designed to investigate the solubilities of inorganic compounds in supercritical water. In this work, three alkali chloride salts (LiCl, NaCl, KCl) and three alkali nitrate salts ($LiNO_3$, $NaNO_3$, KNO_3) were investigated in the range from (653 to 693) K and from (18 to 23.5) MPa. The experimental results were correlated with a model based on the phase equilibrium between the inorganic compound and supercritical water. When available, the experimental data were extended with data available in the open literature. The experimental results and parameters obtained by this model were compared with each other and evaluated under consideration of the physical aspects of the inorganic compounds. In addition to the main purpose of the experiments, side reactions like decomposition of nitrate and changes in pH were observed and discussed in this work. The presented data are the first coherent study of the solubility of six common inorganic compounds in one setup and with one method.

Introduction

Supercritical fluids receive more and more attention in science and industry due to the versatile application possibilities. This versatility is based on the adjustable properties of supercritical fluids.[1] The applications for supercritical fluids range from extraction, particle formation, reactions, and cleaning to dyeing.[2−10]

Supercritical water as a medium for industrial applications has received little attention in the literature and research so far since the critical properties ($T_c = 647$ K, $p_c = 22.1$ MPa) result in harsher conditions for materials and equipment. This results in limited knowledge of the properties of supercritical water systems and mixtures of supercritical water and organic/inorganic compounds compared to other fluids (e.g., carbon dioxide). Nevertheless, several new approaches and research projects recently started to use supercritical water as a solvent of choice due to the beneficial aspects of supercritical water (e.g., inexpensive and green solvent, high thermal capacity, diffusion adaptability, changing solvation behavior). These projects include reactions in supercritical water,[11−14] gasification of biomass in supercritical water,[15−17] oxidation of waste material in supercritical water,[18−21] and the removal of inorganic compounds in supercritical water. To improve and to optimize these new approaches, additional data and understanding of the system is necessary.[22]

One important aspect for all these approaches is the presence of inorganic compounds (e.g., salts) in the supercritical system. The solubility of these compounds is tremendously diminished in comparison to the solubility at ambient conditions.[23,24] The reason for this is the different structure of supercritical water and the reduced dielectric constant. This leads to weaker hydrogen bonding and to less hydration of the inorganic molecules by the surrounding water molecules.[25,26] Due to this behavior, water changes from an excellent solvent for inorganic compounds at ambient conditions to a poor one at supercritical conditions. As a result of the diminished solubility, the inorganic compounds start to precipitate and to form a solid phase within the supercritical water system.

The presence of a solid phase may lead to problems within the system. Blocking of parts of the equipment may occur as well as the deposition of solid particles on the walls of the equipment.[27−29] This can result in an increased pressure drop along the system and end up in a total failure. Additionally, erosion and corrosion are negative side effects of the presence of a solid phase, especially if the material used is not designed or capable to deal with corrosion.[30−33] On the other hand, the diminished solubility of inorganic compounds can be used to remove these compounds from the water phase, or the different solubilities of different salts can be applied to separate the salt fractions from each other.

To obtain further insight into the properties of salt + supercritical water systems, three alkali nitrate salts ($LiNO_3$, $NaNO_3$, KNO_3) and three alkali chloride salts (LiCl, NaCl, KCl) were investigated systematically regarding their solubility and behavior. The investigated temperature and pressure range was (653 to 693) K and from (18 to 23.5) MPa. These two sets differ in the type of the cation. The effect of the type of cation and anion was studied by comparison of the experimental results. The results of the experiments were evaluated using a model based on the description of the phase equilibrium between the solid phase and the supercritical fluid phase.[34,35] The parameters obtained with this model are compared, and a correlation between these parameters and the properties of the solids is proposed. Furthermore, several aspects like possible side

* To whom correspondence should be addressed. E-mail: ingo.leusbrock@wetsus.nl.
† Wetsus.
‡ Procede.
§ University of Groningen.

10.1021/je900175b CCC: $40.75
Published on Web 07/30/2009

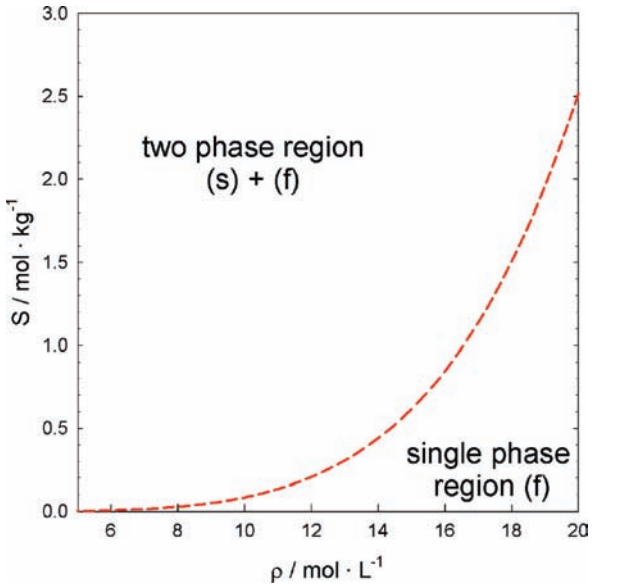

Figure 1. Solubility curve of NaCl.[24]

reactions during the experiments as well as changes in pH are mentioned and discussed.

Theoretical Background

Solubility in Supercritical Water. For the interpretation of the solubility experiments, a model derived from the description of the equilibrium between the two present phases, solid and supercritical fluid, is applied.[24,35−37] A phase diagram with the solubility of NaCl as a function of the density of water is shown in Figure 1. This equilibrium can be interpreted as follows

$$a \cdot \mathrm{Me}^{c} \cdot m \cdot \mathrm{H_2O(f)} + b \cdot \mathrm{X}^{d} \cdot p \cdot \mathrm{H_2O(f)} \rightleftharpoons \mathrm{Me}_a\mathrm{X}_b \cdot n \cdot \mathrm{H_2O(f)} \quad (1)$$

$$\mathrm{Me}_a\mathrm{X}_b \cdot n \cdot \mathrm{H_2O(f)} \rightleftharpoons \mathrm{Me}_a\mathrm{X}_b\mathrm{(s)} + n \cdot \mathrm{H_2O(f)} \quad (2)$$

Me represents the salt cation, while X represents the salt anion; a and b are the number of ions in the salt molecule, and c and d are its valency. n, m, and p are the number of water molecules needed for solvation for the salt and the ions, while s and f refer to the phases solid and fluid. Regarding the equilibrium, it is assumed that the formation of a solid only takes place via the associated complex and not via the dissociated salt ions.

A formulation of the phase equilibrium constant K_s leads to the following expression

$$K_s = \frac{\alpha_{\mathrm{Me}_a\mathrm{X}_b \cdot n \cdot \mathrm{H_2O(f)}}}{\alpha_{\mathrm{Me}_a\mathrm{X}_b\mathrm{(s)}} \cdot \alpha^{n}_{\mathrm{H_2O(f)}}} \quad (3)$$

α refers to the activity of the species on a molality base.

Several assumptions can be made to simplify this expression. The activity coefficient of the solid salts is considered as unity. Interaction between the presented species is neglected. For the fluid water phase, an ideal behavior is assumed. These assumptions have been used successfully to describe the solubility of inorganic compounds in supercritical fluids.[24,34,35]

For a more convenient interpretation of the parameters, a description on an amount of substance base is chosen. The density of water is described as the amount of substance density, while the composition is given as molality. The density of pure water is calculated via the IAPWS95 equation of state.[38]

A more detailed explanation on the assumptions can be found in a previous work of the authors.[34]

$$K^{*}_{s} \approx \frac{m_{\mathrm{Me}_a\mathrm{X}_b \cdot n \cdot \mathrm{H_2O(f)}}}{1 \cdot \rho^{n}_{m,\mathrm{H_2O(f)}}} \quad (4)$$

$$\Rightarrow m_{\mathrm{Me}_a\mathrm{X}_b \cdot n \cdot \mathrm{H_2O(f)}} = K^{*}_{s} \cdot \rho^{n}_{m,\mathrm{H_2O(f)}} \quad (5)$$

The equilibrium constant for the simplified form of the equilibrium, K^{*}_{s}, can be also expressed under usage of a van't Hoff like expression as

$$K^{*}_{s} = \exp\left(-\frac{\Delta_{\mathrm{solv}}G}{R \cdot T}\right) \quad (6)$$

$$= \exp\left(-\frac{\Delta_{\mathrm{solv}}H}{R \cdot T} + \frac{\Delta_{\mathrm{solv}}S}{R}\right) \quad (7)$$

$$\Rightarrow \log m_{\mathrm{Me}_a\mathrm{X}_b \cdot n \cdot \mathrm{H_2O}} = \log K^{*}_{s} + n \cdot \log \rho_{m,\mathrm{H_2O}} \quad (8)$$

$$= -\frac{\Delta_{\mathrm{solv}}H}{R \cdot T} + \frac{\Delta_{\mathrm{solv}}S}{R} + n \cdot \log \rho_{m,\mathrm{H_2O}} \quad (9)$$

R is the universal gas constant; T is the system temperature; and m is the molality. For the Gibbs energy of solvation, $\Delta_{\mathrm{solv}}G$, the enthalpy of solvation, $\Delta_{\mathrm{solv}}H$, and the entropy of solvation, $\Delta_{\mathrm{solv}}S$, it is assumed that they are independent of the system parameters temperature, pressure, and density. n is later on referred to as the coordination number. To indicate the assumption of an independence of the enthalpy of solvation and the entropy of solvation from the system properties, eq 9 is formulated as follows

$$\log m_{\mathrm{Me}_a\mathrm{X}_b \cdot n \cdot \mathrm{H_2O}} = -\frac{A}{R \cdot T} + \frac{B}{R} + n \cdot \log \rho_{m,\mathrm{H_2O}} \quad (10)$$

The validity and the applicability of this approach for the interpretation of the salt + supercritical water system has been shown elsewhere.[34] In this previous work, eq 9, respectively, eq 10 has been compared and evaluated to several further approaches from the literature.

Experimental Section

Experimental Setup. For the measurement of the solubilities, an experimental setup was designed (cf. Figure 2). The operation range of the setup is up to 25 MPa as well as up to 723 K. To avoid corrosion and to guarantee to withstand the mechanical and thermal stress of the conditions, Hastelloy is used for all parts that are in contact with the heated medium. The pressure is provided by an HPLC pump (LabAlliance Series III) with a volume flow of (0.1 to 10) mL·min^{-1}. The temperature is provided by a custom-made oven which is supported by an electrical preheater. Inside the oven, a U-tube is installed in which the precipitation takes place. The inner diameter of the tube is 4.6 mm, the outer diameter 6.35 mm, and the length 265 mm. The temperature along this tube is measured at three different positions with standard PT100 thermocouples (relative uncertainty 0.25 %). The pressure inside the setup is measured with a pressure sensor (Keller PA23H, relative uncertainty 0.2 %). Behind the tube, a filter (Pore size 0.5 μm) is installed to prevent any particles from being entrained to later sections. The analysis of the samples is done via an inductive coupled plasma atom emission spectrometer (Perkin-Elmer Optima 5300DV, relative uncertainty < 2 % for all investigated species) for the

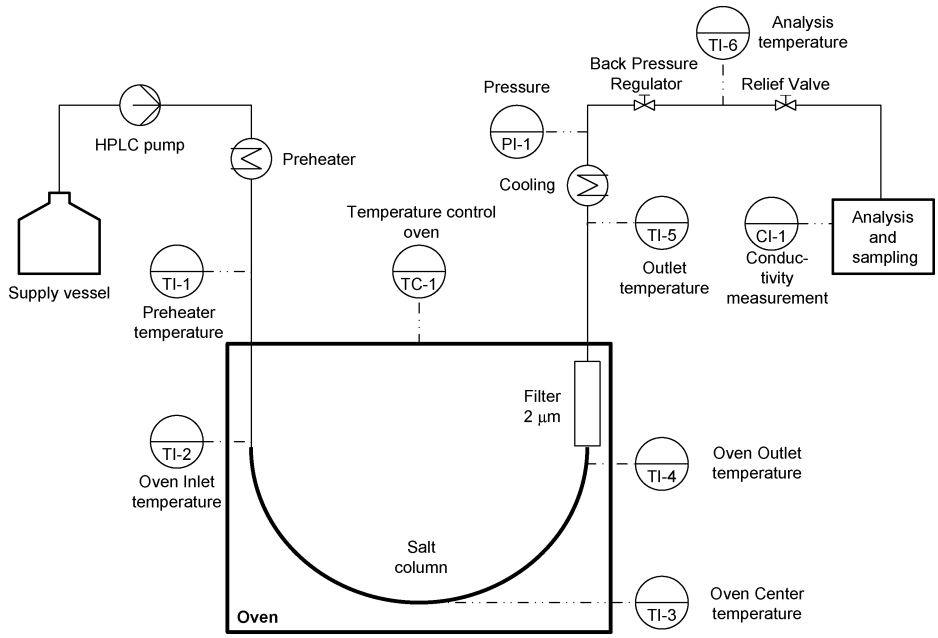

Figure 2. Flow scheme of the experimental setup.

cation composition and liquid chromatography (Metrohm 741 Compact IC, relative uncertainty < 5 % for all investigated species) for the anion composition. The pH values of the samples were measured with a standard pH electrode (WTW pH/Cond 340i/SET; uncertainty after calibration ± 0.01). The process data are logged continuously for later interpretation of the results.

Experimental Procedure. As a feed stream, deionized water plus a known amount of salt were used. The salts that were used were of high purity (> 99.5 %). The salt concentration in the feed was 0.05 mol·L^{-1}. The volume flow was 1 mL·min^{-1} for the experiments with NaCl, for the other salts 0.5 mL·min^{-1}. The resulting residence time was approx. 260 s, respectively, 520 s. The temperature and pressure in the column were adjusted to the desired conditions. The temperature was kept constant for the duration of the whole experiment, while the pressure was reduced stepwise after taking samples at each measurement point.

Upon entering the column, the stream can be oversaturated due to the conditions in the column and the investigated salt. If an oversaturation occurs, precipitation of the salt will take place until the phase equilibrium between both phases is established in the column. The resulting stream leaves the system at the solubility resulting from the temperature and pressure in the column. The stream is cooled down and depressurized to ambient conditions.

Next to the other properties, the conductivity of the outlet stream is measured. If the conductivity and thereby the composition was constant for a longer period of time ($t \geq 10$ min), an equilibrium state in the column was assumed. If the system reaches such a constant state, two samples were taken in an interval of 30 min. These samples are analyzed regarding their composition with the analytical methods mentioned above. For the calculation of the density, the outlet temperature (TI-4 in Figure 2) and the pressure at the pressure sensor (PI-1 in Figure 2) were used. Pressure drops between the U-tube and the pressure sensor were neglected due to the low volume flows. Plugging inside in the U-tube was avoided by the low feed concentration and the (in comparison, the feed concentration) large volume of the U-tube.

Table 1. Properties of $LiNO_3$, $NaNO_3$, and KNO_3

Salt	T_{fus}/K[39]	M/g·mol^{-1}[39]	r/10^{-12} m[40]
$LiNO_3$	537	68.95	352
$NaNO_3$	580	84.99	392
KNO_3	607	101.11	430

A more extensive description of the setup and the procedure can be found elsewhere.[34]

Results and Discussion

To increase the available property data of inorganic compounds in supercritical water, two sets of salts were systematically investigated, alkali nitrate and chloride salts. Each set is distinguished by the type of cation: lithium, sodium, and potassium. Each salt was investigated regarding its solubility with the same setup and method. For several of these salts, almost no literature data were available until this point.

Nitrate Salts. Three alkali nitrate compounds were investigated: $LiNO_3$, $NaNO_3$, and KNO_3. Several properties of these salts are listed in Table 1.[39,40] The molecule radius is the sum of the crystal radius of the anion and the cation.[40] The melting temperatures of all nitrates are below the investigated temperature range resulting in the nitrate salts being in a liquid state during the experiments.

In Figure 3, Figure 4, and Figure 5, the experimental data on the different nitrate salts are presented. The solubility of each compound is presented as a function of the density of pure water, thereby as a function of temperature and pressure. The experimental data cover a density range of (4 to 9) mol·L^{-1} (approx. (17 to 23.5) MPa, (650 to 700) K). Where available, solubility data from the literature were added to the experimental data.[41] As can be seen from the figures, the measurements presented in this work agree well with the results in the literature. The experimental data including temperature and pressure as well as their standard deviations, the density, the composition, and the pH for the measurements on the nitrate salts can be found in the Supporting Information.

The three parameters of eq 10, A, B, and n, were fitted to the experimental data by application of the software MATLAB. For the fitting procedure, the cation composition was used as

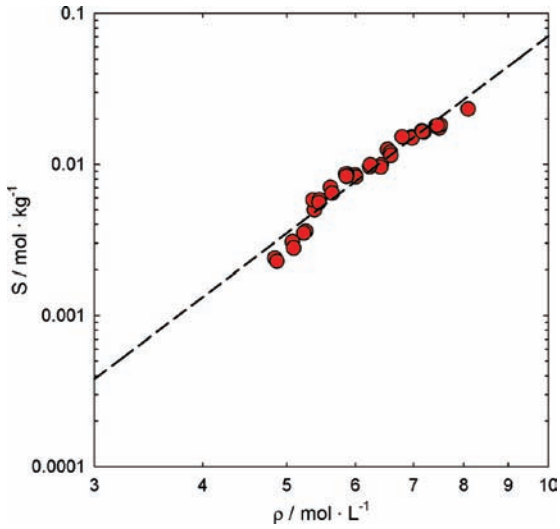

Figure 3. S($LiNO_3$): ●, this work; dashed line represents the description of the experimental data with eq 10; parameters are listed in Table 2.

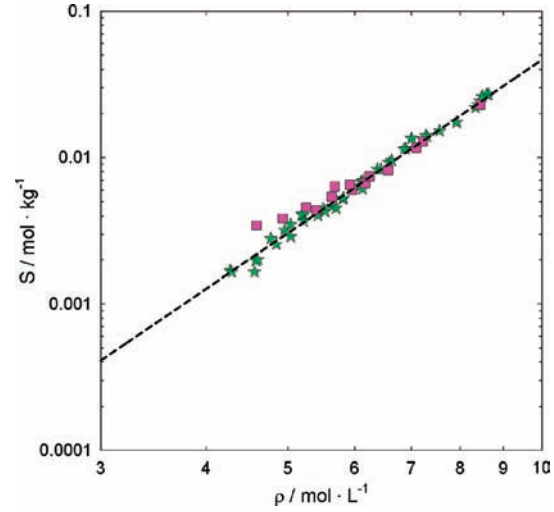

Figure 4. S($NaNO_3$): ★, this work; ■, Dell'Orco et al.;[41] dashed line represents the description of the experimental data with eq 10; parameters are listed in Table 2.

solubility in consistence with previous works.[24,34,42] All experimental data can be described with good agreement with the model presented.[34] The obtained parameters for this model are listed in Table 2 and will be discussed in the following section.

Chloride Salts. Three alkali chloride compounds were investigated: LiCl, NaCl, and KCl. Several properties of these salts are listed in Table 3.[39,40]

In Figure 7, Figure 8, and Figure 9, the experimental data on the different nitrate salts are presented. The solubility of each compound is presented as a function of the density of pure water, thereby as a function of temperature and pressure. The experimental data cover a density range of (4 to 9) mol·L^{-1} (approx. (17 to 23.5) MPa, (650 to 700) K). Where available, solubility data from the literature were added to experimental data from this work.[24,42,43] As can be seen from the figures, the measurements presented in this work agree well with the results in the literature. The experimental data for the measurements on the chloride salts can be found in the Supporting Information. The experimental data for NaCl can also be found in Table 6. For the measurements of NaCl, a scatter in the solubility results has to be mentioned.

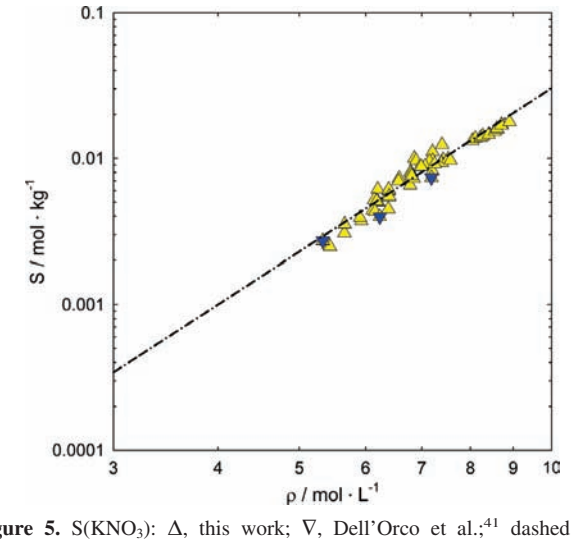

Figure 5. S(KNO_3): Δ, this work; ∇, Dell'Orco et al.;[41] dashed line represents the description of the experimental data with eq 10; parameters are listed in Table 2.

Table 2. Parameters for the Description of the Solubilities of $LiNO_3$, $NaNO_3$, and KNO_3 with Equation 10

Salt	A/J·mol^{-1}	B/J·mol^{-1}·K^{-1}	n
$LiNO_3$	15594	−81.91	4.33
$NaNO_3$	5149	−93.06	3.93
KNO_3	−7793	−111.91	3.72

Table 3. Properties of LiCl, NaCl, and KCl

Salt	T_{fus}/K[39]	M/g·mol^{-1}[39]	$r/10^{-12}$ m[40]
LiCl	886	42.4	240
NaCl	1074	58.45	280
KCl	1049	74.55	318

All experimental data can be described with good agreement with the presented model. The parameters obtained with this model are listed in Table 4.

Side Reactions in SCW. In all experiments with nitrate salts, a small amount of nitrite was found in the samples. Since the feed solutions were produced by using very pure nitrate salts, it can be assumed that a decomposition of nitrate to nitrite took place.

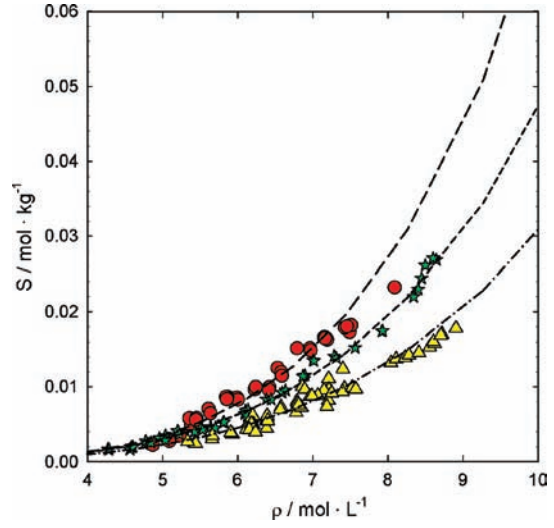

Figure 6. Comparison of the solubilities of $LiNO_3$, $NaNO_3$, and KNO_3: ●, $LiNO_3$; ★, $NaNO_3$; Δ, KNO_3; dashed lines represent the respective description of the solubilities with eq 10.

$$2XNO_3 \rightleftharpoons 2XNO_2 + O_2 \quad (11)$$

The molality of nitrite in the experiments with $LiNO_3$,$NaNO_3$, and KNO_3 was determined as between (0.0005 and 0.0015) mol·kg^{-1}. These results on the nitrite composition show a relatively experimental high uncertainty (multiple analyses of the same sample showed deviations in the range of 10 % in nitrite composition from each other; this was caused by operating at the lower end of the detection limit of the analytical method) due to the low concentrations. Yet the qualitative result of these observations, the decomposition from nitrate to nitrite, is without doubt. Although only a rather small temperature range from (650 to 700) K was investigated, a higher decomposition of nitrate to nitrite can be expected at higher temperatures. Especially, the presence of oxygen might lead to problems in applications since corrosion is enhanced by the presence of oxygen.

In all experiments, a decrease in pH from 4 to 6 was measured. Due to the only slightly acidic feed solutions, pH 6.7 to 6.9, for all salts, a hydrolysis of the salt is considered as the reason for the drop in pH.[24,41,43] The equilibrium of the hydrolysis is favorable to higher temperatures/lower densities (cf. Figure 11). The possible reaction mechanism is depicted below

$$XCl + H_2O \rightleftharpoons XOH(s)\downarrow + HCl \quad (12)$$

$$XNO_3 + H_2O \rightleftharpoons XOH(s)\downarrow + HNO_3 \quad (13)$$

The hydroxide precipitates and remains in the column. From this reaction, the outlet stream becomes acidic due to the presence of HCl/HNO_3. This fact is supported by the ratio of the cation and the anion concentrations in the samples. Here the ratio of anion to cation is usually slightly higher than 1 which indicates a surplus of anions due to the hydrolysis. Therefore, the cation composition of the outlet stream corresponds to the solubility of the investigated salt if the hydrolysis is taken into account. Yet the pH change is small resulting in small differences between the anion and cation composition. This decrease in pH for all salt solutions has to be kept in mind for applications where corrosion must be prevented, and the water stream is used afterward for further purposes.

During the evaluation of the experimental data, the side reactions have been not accounted and corrected for. It is assumed that at pH 4 a maximum deviation in the solubility of 5 % results due to the side reactions.

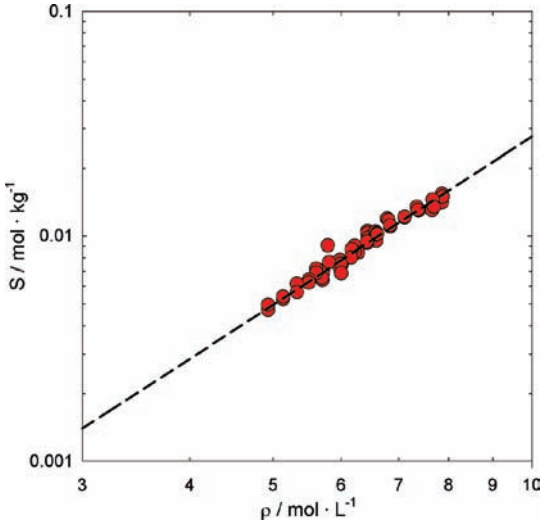

Figure 7. S(LiCl): ●, this work; dashed line represents the description of the experimental data with eq 10; parameters are listed in Table 4.

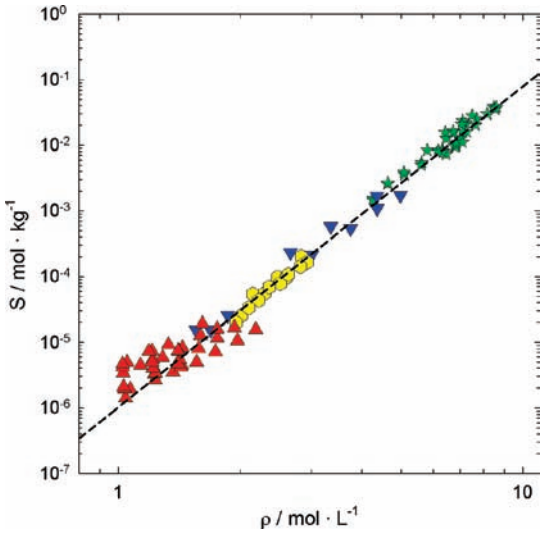

Figure 8. S(NaCl): ★, this work; ∇, Armellini et al.;[24] ⬢, Higashi et al.;[42] Δ, Galobardes et al.;[43] dashed line represents the description of the experimental data with eq 10; parameters are listed in Table 4.

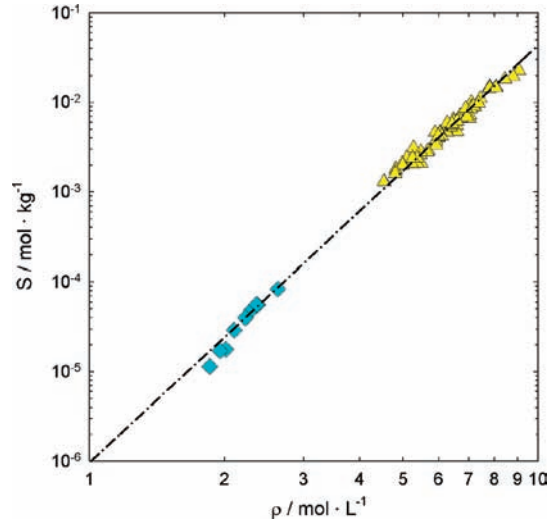

Figure 9. S(KCl): Δ, this work; ◇, Higashi et al.;[42] dashed line represents the description of the experimental data with eq 10; parameters are listed in Table 4.

Table 4. Parameters for the Description of the Solubilities of LiCl, NaCl, and KCl with Equation 10

Salt	A/J·mol^{-1}	B/J·mol^{-1}·K^{-1}	n
LiCl	5199	−69.61	2.48
NaCl	18784	−86.74	4.88
KCl	13123	−95.66	4.65

Table 5. Model Parameters of the Salts CuO, PbO, and KOH for Equation 10[37,48,49]

Salt	A/J·mol^{-1}	B/J·mol^{-1}·K^{-1}	n
CuO	23749	−103.68	1.339
PbO	27901	−57.97	1.971
KOH	13369	−81.10	3.244

Discussion

In Figure 6, the solubilities of the nitrate salts are compared. A trend in the solubilities can be clearly seen so that a tendency in the solubility of alkali nitrate salts can be determined ($LiNO_3$ > $NaNO_3$ > KNO_3). This tendency has also been assumed by

Table 6. Experimental Results of NaCl[a]

T/K		σT/K	p/MPa		σp/MPa	ρ/mol·L^{-1}	c(Na$^+$)/mmol·kg^{-1}	pH
654.11	±	0.45	22.55	±	0.02	9.84	87	5.96
656.17	±	0.46	22.33	±	0.02	8.90	48.68	5.80
666.79	±	0.75	23.54	±	0.02	8.60	38.26	5.24
656.92	±	0.44	22.15	±	0.01	8.51	35.64	5.59
657.00	±	0.44	22.15	±	0.01	8.49	38.6	5.74
666.27	±	0.47	23.07	±	0.02	8.18	29.85	5.08
673.23	±	0.55	23.10	±	0.02	7.49	28.39	5.72
672.89	±	0.55	23.27	±	0.02	7.66	25.28	5.35
673.38	±	0.58	23.29	±	0.02	7.62	20.37	5.57
675.45	±	0.58	23.03	±	0.01	7.26	16.01	5.13
672.02	±	0.54	22.60	±	0.02	7.21	21.39	4.93
673.42	±	0.59	22.61	±	0.02	7.12	15.91	4.64
674.25	±	0.65	22.68	±	0.02	7.10	23.48	5.02
674.77	±	0.51	22.73	±	0.02	7.10	11.14	5.08
675.15	±	0.65	22.72	±	0.02	7.07	20.93	5.01
678.92	±	0.57	23.03	±	0.01	7.02	12.61	5.25
679.13	±	0.59	23.02	±	0.01	7.00	12.58	5.08
676.25	±	0.61	22.51	±	0.01	6.86	10.88	5.02
676.62	±	0.60	22.51	±	0.01	6.83	10.23	5.49
683.87	±	0.61	23.23	±	0.02	6.83	9.65	5.28
684.48	±	0.61	23.20	±	0.01	6.79	9.61	5.26
678.74	±	0.65	22.55	±	0.02	6.73	15.35	5.17
678.43	±	0.56	22.54	±	0.02	6.74	16.39	n.a.
667.13	±	0.47	21.02	±	0.01	6.46	12.66	4.64
681.64	±	0.66	22.37	±	0.02	6.46	7.32	5.03
667.70	±	0.49	21.03	±	0.01	6.43	15.67	4.61
682.70	±	0.60	22.26	±	0.01	6.35	7.89	4.98
684.02	±	0.62	22.38	±	0.02	6.35	8.16	4.96
683.16	±	0.61	22.26	±	0.01	6.32	8.7	4.88
671.87	±	0.67	21.02	±	0.02	6.20	7.88	4.63
672.14	±	0.68	21.02	±	0.02	6.18	8.44	4.91
674.92	±	0.62	20.58	±	0.02	5.80	8.4	5.28
672.96	±	0.61	20.08	±	0.02	5.63	5.53	4.69
673.04	±	0.58	20.06	±	0.02	5.61	5.05	4.77
673.27	±	0.63	19.01	±	0.02	5.10	3.59	4.65
673.57	±	0.57	19.01	±	0.02	5.09	3.89	4.72
673.42	±	0.60	17.98	±	0.02	4.64	2.68	4.60
673.42	±	0.59	17.95	±	0.02	4.63	2.6	4.67
673.34	±	0.67	17.07	±	0.01	4.28	1.44	4.50
673.72	±	0.62	17.05	±	0.01	4.27	1.53	4.60

[a] σT and σp are the standard deviations of the measured temperature and pressure, respectively, during the experiment.

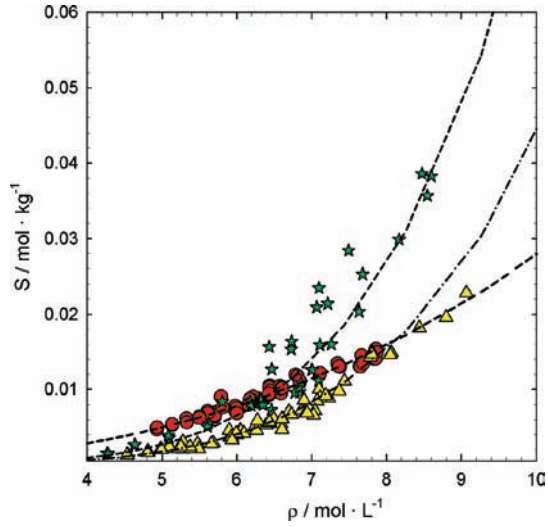

Figure 10. Comparison of the solubilities of LiCl, NaCl, and KCl: ●, LiCl; ★, NaCl; Δ, KCl; dashed lines represent the respective description of the solubilities with eq 10.

other groups, yet the available experimental data were scarce.[41] To explain this tendency, the radii of the salt molecules can be taken into consideration. Due to the changed physical properties

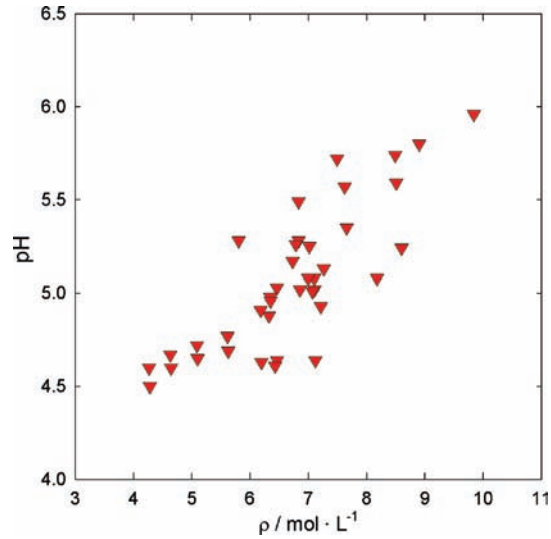

Figure 11. Measured pH of the experiments with NaCl as a function of the density.

of water in its supercritical state and the therefore diminished dielectric constant, the solvation power of water is reduced, and the hydrogen bonds are weakened.[26] As one result, this leads to an association of the ions.[25,34,44] As a further effect, the hydration of the molecules decreases due to the weakened hydrogen bonds.[25,26] Additionally, the hydrogen bonding between the water molecules competes strongly with the actual solvation of the solutes and thereby decreases the solvation ability of supercritical water.[45] As a result, the molecules cannot be kept in solution and start to form a solid phase.

Table 1 contains the radii of the associated nitrate salts with the cation being the only difference. As can be seen from this table and Figure 6, a higher solubility corresponds with a smaller radius. Here, the difficulty in hydration of the salt molecule is considered as a possible reason for this relation. It is easier to maintain the hydration sphere around a smaller molecule and to keep it in solution. This results from the reduced distance between the water molecules to establish hydrogen bondings with other water molecules and the salt molecule and to maintain them.

The parameters of approach in eq 10, A, B, and n, for the investigated nitrate salts are listed in Table 2. The coordination number n decreases from 4.33 for $LiNO_3$ to 3.72 for KNO_3 in correspondence with decreasing solubility and increasing radius. The coordination number can be taken as an indication of how far it is still possible to solvate the salt molecule. If a salt molecule can bind more water molecules in its hydration sphere like $LiNO_3$, its solubility is higher than in comparison with KNO_3. For KNO_3, it is apparent that the larger radius and the changed properties lead to a lower concentration of water molecules around the salt molecule. Therefore, the solubility and the coordination number are lower.

In Figure 10, the solubilities of the chloride salts are compared. The experimental data of NaCl show in comparison to the other salts scatter in the composition results. The experiments on NaCl were the first to be performed with the setup, thereby adding an additional uncertainty. Contrary to the nitrate salts, no clear trend can be seen. While NaCl and KCl behave according to the corresponding nitrate salts, LiCl shows a lower solubility for densities ≥ 6 mol·L^{-1} than one could assume based on the previous results.

A possible explanation for this anomalous behavior is assumed to result from the nature of lithium itself. With lithium

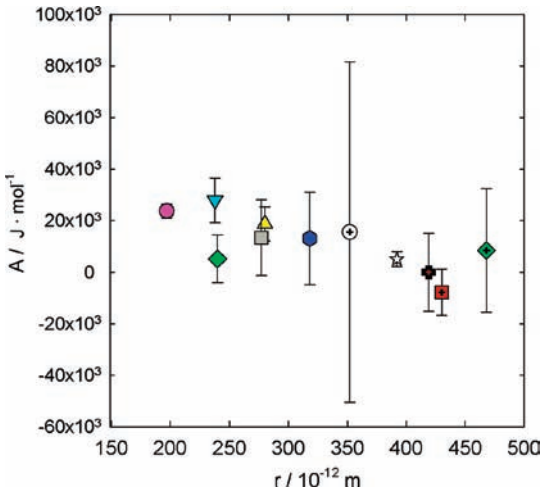

Figure 12. Parameter *A* (cf. eq 10) as a function of the molecule radius: ○, CuO; ∇, PbO; ◇, LiCl; □, KOH; Δ, NaCl; ⬡, KCl; ⊕, $LiNO_3$; ★, $NaNO_3$; ⊞, KNO_3; the vertical bars represent the numerical uncertainty of the parameter resulting from the fitting procedure.

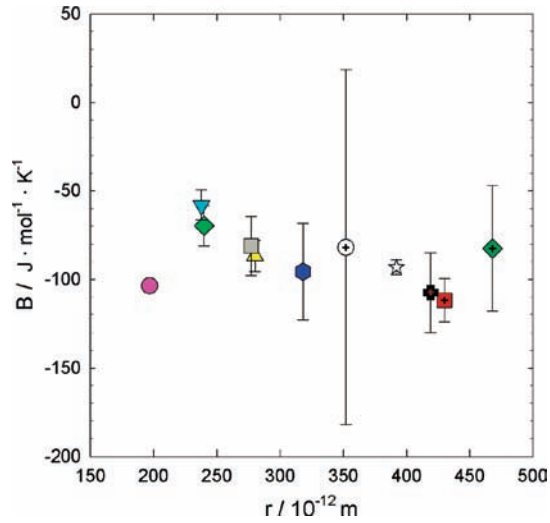

Figure 13. Parameter *B* (cf. eq 10) as a function of the molecule radius: ○, CuO; ∇, PbO; ◇, LiCl; □, KOH; Δ, NaCl; ⬡, KCl; ⊕, $LiNO_3$; ★, $NaNO_3$; ⊞, KNO_3; the vertical bars represent the numerical uncertainty of the parameter resulting from the fitting procedure.

being the lightest of the metals and having the smallest ionic radius, several abnormal phenomena in comparison to other alkali metals exist (e.g., diagonal relationship with magnesium, high solubility in polar organic solvents).[46] Due to the small ionic radius, the lithium cation has a high charge density which results in a stronger attraction of the electrons of the corresponding anion. Therefore, considering the proposed association and precipitation mechanism (cf. eq 2), the formed associated LiCl complex is likely to have a more covalent bonding structure than the NaCl and KCl complex. This results in a more difficult hydration and a lower solubility for LiCl since partial charges of the molecules are not as pronounced as for NaCl and KCl. Nevertheless, this does not explain the higher solubilities of LiCl in comparison to NaCl and KCl at lower densities. To investigate the actual hydration structure of LiCl and compare it to NaCl and KCl, molecular modeling and spectrographic measurements (Infrared, Raman)[47] are considered as possible tools. The application of these tools could give a verification of the assumptions made above or offer a different explanation for this phenomenon.

Relation of Model Parameters and Salt Properties. Due to the results presented above, a possible relation between the radius of the salt molecule and the model parameters of eq 10 is investigated. To extend the available data and to have a greater significance, parameters of three additional monovalent salts (CuO, PbO, KOH) are added to the parameters presented in the section before. These parameters were obtained from solubility data available in the literature[37,48,49] and can be found in Table 5. The experimental data[48] for CuO have to be treated carefully since large scattering occurs throughout the data set.

In Figure 12, Figure 13, and Figure 14, the model parameters are presented as a function of the molecule radius including the standard deviations (cf. Table 2 and Table 4). The radii were obtained from the corresponding crystal radii.[40] For the parameter *A*, which is a direct function of the temperature, and *B*, which is correlated to the parameter ΔH due to the chosen mathematical approach (cf. eq 10), the magnitudes of the standard deviations are primarily resulting from the temperature range that is covered in the experimental data. This is most prominent for $LiNO_3$ where only a range from (663 to 679) K was investigated. Therefore, additional experiments for $LiNO_3$ are advisible to correct these deviations.

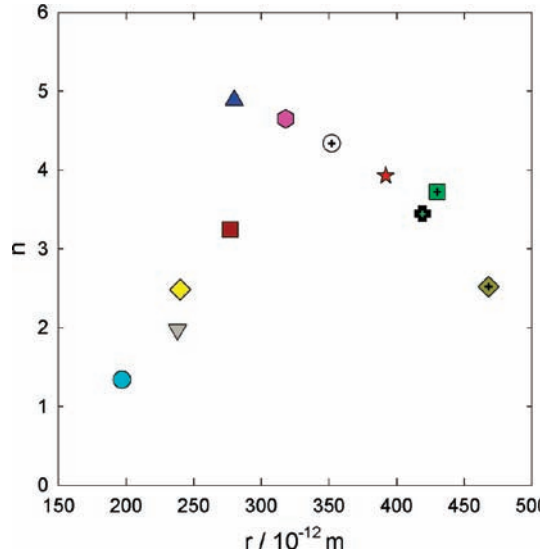

Figure 14. Parameter *n* (cf. eq 10) as a function of the molecule radius: ○, CuO; ∇, PbO; ◇, LiCl; □, KOH; Δ, NaCl; ⬡, KCl; ⊕, $LiNO_3$; ★, $NaNO_3$; ⊞, KNO_3; the vertical bars represent the numerical uncertainty of the parameter resulting from the fitting procedure.

For the parameters *A* and *B*, a linear correlation between the radius and the parameter can be found. Both parameters increase with decreasing radius.

For the parameter *n*, two groups can be distinguished (group I: NaCl, KCl, $LiNO_3$, $NaNO_3$, KNO_3; group II: CuO, PbO, LiCl, KOH). Group I shows a linear correlation with an increasing coordination number for a smaller molecule radius. This behavior has been discussed above for the nitrate salts in regard to the overall solubility, where the coordination number was taken as an indicator for the solubility. As can be seen in Figure 14, this behavior can also be found for KCl and NaCl.

Group II shows a different tendency. Their coordination number shows an increasing trend with an increasing radius. CuO, PbO, KOH, and LiCl (as discussed above) have a more covalent binding character in comparison to the more ionic compounds in group I. Therefore, the difference in electronegativity between the salt components can be taken as an indicator for ionic/covalent character (e.g., difference in electronegativity

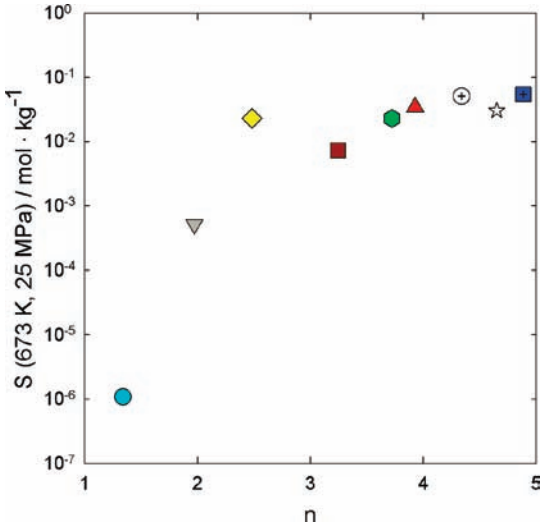

Figure 15. Solubility at 673 K and 25 MPa as a function of the coordination number: ○, CuO; ▽, PbO; ◇, LiCl; □, KOH; ○, $NaNO_3$; △, KNO_3; ⊕, $LiNO_3$; ★, KCl; ⊞, NaCl.

of NaCl: 3.16 (Cl); 0.93 (Na); difference in electronegativity of CuO: 3.44 (O); 1.90 (Cu)). The more covalent character results in less pronounced local charges which makes it more difficult to establish hydrogen bonds between the salt molecule and the surrounding water. Therefore, less water molecules are bound to the salt molecule resulting in a lower coordination number. It can be concluded from this behavior that the coordination number is depending not only on the molecule radius but also on the binding character of the compound.

In Figure 15, the solubilities of the salts mentioned above at 673 K and 25 MPa are presented as a function of the coordination number. As can be seen, increasing solubility correlates in an exponential manner with an increasing coordination number (with the exception of CuO). Therefore, these relations between the radius, the binding character, and the parameters of the model can be used to predict to a certain degree the solubilities of salts and the parameters of the model where no or little property data are available in the open literature.

Conclusions

In the course of this work, a systematic study of the solubilities of three alkali chloride salts (LiCl, NaCl, KCl) and three alkali nitrate salts ($LiNO_3$, $NaNO_3$, KNO_3) was performed. The study was performed in one setup using one method. The investigated range was from (653 to 693) K and from (18 to 23.5) MPa.

The solubilities of each group were compared with each other. For alkali nitrates, a clear tendency in the solubility in correspondence with the molecule radius could be determined ($LiNO_3$ > $NaNO_3$ > KNO_3). For alkali chlorides, a similar tendency could not be determined due to the anomalous behavior of LiCl. Considering the parameters obtained from the model, it can be concluded that a high solubility in supercritical water correlates with the ability of the molecule to establish as many hydrogen bonds with the surrounding water and to maintain a hydration sphere. This results in a higher coordination number.

A comparison of the radii of the inorganic compounds with the parameters obtained by eq 10 showed that a linear relation exists between the enthalpy and entropy parameter and the radius. The coordination number was found to be additionally depending on the binding character of the molecule.

The experiments revealed that next to the precipitation of alkali chlorides and nitrates several side reactions take place. During all experiments a drop in pH from 4 to 6 was found resulting from a hydrolysis reaction. During the experiments with alkali nitrates, small concentrations of nitrite were found resulting from the decomposition of the nitrate.

Acknowledgment

The authors thank Sonia Touzot for her contribution to the experimental part of this work. Additionally, the authors thank Janneke Tempel and Jelmer Dijkstra for their contribution in the analysis of the samples.

Supporting Information Available:

The experimental data for the measurements of the solubilities of three alkali chloride salts (LiCl, NaCl, KCl) and three alkali nitrate salts ($LiNO_3$, $NaNO_3$, KNO_3). This material is available free of charge via the Internet at http://pubs.acs.org.

Literature Cited

(1) Clifford, T. *Fundamentals of Supercritical Fluids*; Oxford University Press, 1999.
(2) Aymonier, C.; Loppinet-Serani, A.; Reveron, H.; Garrabos, Y.; Cansell, F. Review of supercritical fluids in inorganic materials science. *J. Supercrit. Fluids* **2006**, *38*, 242–251.
(3) Cansell, F.; Rey, S.; Beslin, P. Continous catalytic reactions in supercritical fluids processing: Applications to polymers and waste treatment. *Rev. Inst. Fr. Pet.* **1998**, *1*, 71–98.
(4) Erkey, C. Supercritical carbon dioxide extraction of metals from aqueous solutions: a review. *J. Supercrit. Fluids* **2000**, *17*, 259–287.
(5) Fages, J.; Lochard, H.; Letourneau, J.-J.; Sauceau, M.; Rodier, E. Particle generation for pharmaceutical applications using supercritical fluid technology. *Powder Technol.* **2004**, *141*, 219–226.
(6) Hyde, J. R.; Licence, P.; Carter, D.; Poliakoff, M. Continuous catalytic reactions in supercritical fluids. *Appl. Catal., A* **2001**, *222*, 119–131.
(7) Jarzebski, A. B.; Malinowski, J. J. Potentials and Prospects for Application of Supercritical Fluid Technology in Bioprocessing. *Process Biochem.* **1995**, *30*, 343–352.
(8) Jung, J.; Perrut, M. Particle design using supercritical fluids: Literature and patent survey. *J. Supercrit. Fluids* **2001**, *20*, 179–219.
(9) van der Kraan, M.; Fernandez Cid, M. V.; Woerlee, G. F.; Veugelers, W.; Witkamp, G.-J. Dyeing of natural and synthetic textiles in supercritical carbon dioxide with disperse reactive dyes. *J. Supercrit. Fluids* **2007**, *40*, 470–476.
(10) van Roosmalen, M. J.; van Diggelen, M.; Woerlee, G. F.; Witkamp, G.-J. Dry-cleaning with high-pressure carbon dioxide-the influence of mechanical action on washing-results. *J. Supercrit. Fluids* **2003**, *27*, 97–108.
(11) Kruse, A.; Dinjus, E. Hot compressed water as reaction medium and reactant: Properties and synthesis reactions. *J. Supercrit. Fluids* **2007**, *39*, 362–379.
(12) Lester, E.; Blood, P.; Denyer, J.; Giddings, D.; Azzopardi, B.; Poliakoff, M. Reaction engineering: The supercritical water hydrothermal synthesis of nano-particles. *J. Supercrit. Fluids* **2006**, *37*, 209–214.
(13) Savage, P. E. Heterogeneous catalysis in supercritical water. *Catal. Today* **2000**, *62*, 167–173.
(14) DiLeo, G.; Savage, P. E. Catalysis during methanol gasification in supercritical water. *J. Supercrit. Fluids* **2006**, *39*, 228–232.
(15) Antal, M. J.; Allen, S. G.; Schulman, D.; Xu, X.; Divilio, R. J. Biomass Gasification in Supercritical Water. *Ind. Eng. Chem. Res.* **2000**, *39*, 4040–4053.
(16) Feng, W.; van der Kooi, H. J.; de Swaan Arons, J. Biomass conversions in subcritical and supercritical water: driving force, phase equilibria, and thermodynamic analysis. *Chem. Eng. Process.* **2004**, *43*, 1459–1467.
(17) Matsumura, Y.; Minowa, T.; Potic, B.; Kersten, S. R. A.; Prins, W.; van Swaaij, W. P. M.; van de Beld, B.; Elliott, D. C.; Neuenschwander, G. G.; Kruse, A.; Antal, M. J. Biomass gasification in near- and supercritical water: Status and prospects. *Biomass Bioenergy* **2005**, *29* (269−292), 0961–9534.
(18) Gloyna, E. F.; Li, L. Supercritical water oxidation: an engineering update. *Waste Manage. (Oxford)* **1993**, *13*, 379–394.
(19) Schmieder, H.; Abeln, J. Supercritical water oxidation: state of the art. *Chem. Eng. Technol.* **1999**, *22*, 903–908.

(20) Veriansyah, B.; Park, T.-J.; Lim, J.-S.; Lee, Y.-W. Supercritical water oxidation of wastewater from LCD manufacturing process: kinetic and formation of chromium oxide nanoparticles. *J. Supercrit. Fluids* **2005**, *34*, 51–61.
(21) Prikopsky, K.; Wellig, B.; von Rohr, P. R. SCWO of salt containing artificial wastewater using a transpiring-wall reactor: Experimental results. *J. Supercrit. Fluids* **2007**, *40*, 246–257.
(22) Lummen, N.; Kvamme, B. Kinetics of NaCl nucleation in supercritical water investigated by molecular dynamics simulations. *PCCP* **2007**, *9*, 3251–3260.
(23) Knox, D. E. Solubilities in supercritical fluids. *Pure Appl. Chem.* **2005**, *77*, 513–530.
(24) Armellini, F. J.; Tester, J. W. Solubility of sodium chloride and sulfate in sub- and supercritical water vapor from 450−550 deg.C. and 100−250 bar. *Fluid Phase Equilib.* **1993**, *84*, 123–142.
(25) Yamaguchi, T.; Yamagami, M.; Ohzono, H.; Wakita, H.; Yamanaka, K. Chloride-ion hydration in supercritical water by neutron diffraction. *Chem. Phys. Lett.* **1996**, *252*, 317–321.
(26) Yamaguchi, T. Structure of subcritical and supercritical hydrogen-bonded liquids and solutions. *J. Mol. Liq.* **1998**, *78*, 43–50.
(27) Marrone, P. A.; Hodes, M.; Smith, K. A.; Tester, J. W. Salt precipitation and scale control in supercritical water oxidation-part B: commercial/full-scale applications. *J. Supercrit. Fluids* **2004**, *29*, 289–312.
(28) Hodes, M.; Marrone, P. A.; Hong, G. T.; Smith, K. A.; Tester, J. W. Salt precipitation and scale control in supercritical water oxidation-Part A: fundamentals and research. *J. Supercrit. Fluids* **2004**, *29*, 265–288.
(29) Peterson, A. A.; Vontobel, P.; Vogel, F.; Tester, J. W. In situ visualization of the performance of a supercritical-water salt separator using neutron radiography. *J. Supercrit. Fluids* **2008**, *43*, 490–499.
(30) Kritzer, P.; Boukis, N.; Dinjus, E. Factors controlling corrosion in high-temperature aqueous solutions: a contribution to the dissociation and solubility data influencing corrosion processes. *J. Supercrit. Fluids* **1999**, *15*, 205–227.
(31) Crooker, P. J.; Ahluwalia, K. S.; Fan, Z.; Prince, J. Operating results from supercritical water oxidation plants. *Ind. Eng. Chem. Res.* **2000**, *39*, 4865–4870.
(32) Kritzer, P. Corrosion in high-temperature and supercritical water and aqueous solutions: a review. *J. Supercrit. Fluids* **2004**, *29*, 1–29.
(33) Hayward, T. M.; Svishchev, I. M.; Makhija, R. C. Stainless steel flow reactor for supercritical water oxidation: corrosion tests. *J. Supercrit. Fluids* **2003**, *27*, 275–281.
(34) Leusbrock, I.; Metz, S. J.; Rexwinkel, G.; Versteeg, G. F. Quantitative approaches for the description of solubilities of inorganic compounds in near-critical and supercritical water. *J. Supercrit. Fluids* **2008**, *47*, 117–127.
(35) Chrastil, J. Solubility Of Solids And Liquids In Supercritical Gases. *J. Phys. Chem.* **1982**, *86*, 3016–3021.
(36) Yokoyama, C.; Iwabuchi, A.; Takahashi, S.; Takeuchi, K. Solubility of PbO in supercritical water. *Fluid Phase Equilib.* **1993**, *82*, 323–331.
(37) Sue, K.; Hakuta, Y.; Smith, R. L.; Adschiri, T.; Arai, K. Solubility of Lead(II) Oxide and Copper(II) Oxide in Subcritical and Supercritical Water. *J. Chem. Eng. Data* **1999**, *44*, 1422–1426.
(38) Wagner, W.; Pruss, A. The IAPWS Formulation 1995 for the Thermodynamic Properties of Ordinary Water Substance for General and Scientific Use. *J. Phys. Chem. Ref. Data* **1999**, *31*, 387.
(39) Ride, D. R. *Handbook of Chemistry and Physics*; CRC Press, 2004.
(40) Shannon, R. D. Revised effective ionic-radii and systematic studies of interatmoic distances in halides and chalcogenides. *Acta Crystallogr., Sect. A: Found. Crystallogr.* **1976**, *32*, 751–767.
(41) Dell'Orco, P. C.; Eaton, H.; Reynolds, T.; Buelow, S. The solubility of 1:1 nitrate electrolytes in supercritical water. *J. Supercrit. Fluids* **1995**, *8*, 217–227.
(42) Higashi, H.; Iwai, Y.; Matsumoto, K.; Kitani, Y.; Okazaki, F.; Shimoyama, Y.; Arai, Y. Measurement and correlation for solubilities of alkali metal chlorides in water vapor at high temperature and pressure. *Fluid Phase Equilib.* **2005**, *228−229*, 547–551.
(43) Galobardes, J. F.; Vanhare, D. R.; Rogers, L. B. Solubility of sodium chloride in dry steam. *J. Chem. Eng. Data* **1981**, *26*, 363–366.
(44) Chialvo, A. A.; Cummings, P. T.; Cochran, H. D.; Simonson, J. M.; Mesmer, R. E. Na+ - Cl- ion-pair association in supercritical water. *J. Chem. Phys.* **1995**, *103*, 9379–9387.
(45) Sciáini, G.; Marceca, E.; Fernández-Prini, R. Is Ammonia a Better Solvent Than Water for Contact Ion Pairs? *J. Phys.Chem. B* **2008**, *112*, 11990–11995.
(46) Sapse, A.; Schleyer, P. *Lithium Chemistry: A Theoretical and Experimental Overview*; Wiley-Interscience, 1995.
(47) Tassaing, T.; Garrain, P.; Bégué, D.; Baraille, I. On the cluster composition of supercritical water combining molecular modeling and vibrational spectroscopic data. *Proceedings of the 9th International Symposium on Supercritical Fluids*, 2009.
(48) Hearn, B.; Hunt, M. R.; Hayward, A. Solubility of cupric oxide in pure subcritical and supercritical water. *J. Chem. Eng. Data* **1969**, *14*, 442–447.
(49) Wofford, W. T.; Dell'Orco, P. C.; Gloyna, E. Solubility of potassium hydroxide and potassium phospate in supercritical water. *J. Chem. Eng. Data* **1995**, *40*, 968–973.

Received for review February 23, 2009. Accepted July 17, 2009. This work was performed in the TTIW-cooperation framework of Wetsus, centre of excellence for sustainable water technology (www.wetsus.nl). Wetsus is funded by the Dutch Ministry of Economic Affairs, the European Union Regional Development Fund, the Province of Fryslân, the City of Leeuwarden, and the EZ/Kompas program of the "Samenwerkingsverband Noord-Nederland". The authors would like to thank the participants of the research theme *Salt* for their financial support.

JE900175B